

## Space Weather

### RESEARCH ARTICLE

10.1029/2018SW001988

#### Key Points:

- Sonification can be used for exploratory citizen science, in this case of ultralow-frequency waves at geostationary orbit
- Long-lasting narrowband poloidal field line resonances with decreasing frequency have been identified
- Such events occur more often than previously thought, typically in the recovery phase of geomagnetic storms

#### Supporting Information:

- Supporting Information S1
- Audio S1
- Audio S2
- Audio S3
- Audio S4

#### Correspondence to:

M. O. Archer,  
m.archer@qmul.ac.uk

#### Citation:

Archer, M. O., Hartinger, M. D., Redmon, R., Angelopoulos, V., Walsh, B. M., & Eltham Hill School Year 12 Physics students (2018). First results from sonification and exploratory citizen science of magnetospheric ULF waves: Long-lasting decreasing-frequency poloidal field line resonances following geomagnetic storms. *Space Weather*, 16, 1753–1769. <https://doi.org/10.1029/2018SW001988>

Received 25 JUN 2018

Accepted 19 SEP 2018

Accepted article online 17 OCT 2018

Published online 9 NOV 2018

# First Results From Sonification and Exploratory Citizen Science of Magnetospheric ULF Waves: Long-Lasting Decreasing-Frequency Poloidal Field Line Resonances Following Geomagnetic Storms

M. O. Archer<sup>1,2</sup>, M. D. Hartinger<sup>3</sup>, R. Redmon<sup>4</sup>, V. Angelopoulos<sup>5</sup>, B. M. Walsh<sup>6</sup>, and Eltham Hill School Year 12 Physics Students<sup>7</sup>

<sup>1</sup>School of Physics and Astronomy, Queen Mary University of London, London, UK, <sup>2</sup>Space and Atmospheric Physics Group, Blackett Laboratory, Imperial College London, London, UK, <sup>3</sup>Electrical and Computer Engineering Department, Virginia Tech, Blacksburg, VA, USA, <sup>4</sup>National Oceanic and Atmospheric Administration, Boulder, CO, USA, <sup>5</sup>Department of Earth, Planetary, and Space Sciences, University of California, Los Angeles, CA, USA, <sup>6</sup>Department of Mechanical Engineering and Center for Space Physics, Boston University, Boston, MA, USA, <sup>7</sup>Science Department, Eltham Hill School, London, UK

**Abstract** Magnetospheric ultralow-frequency (ULF) waves contribute to space weather in the solar wind-magnetosphere-ionosphere system. The monitoring of these waves by space- and ground-based instruments, however, produces *big data*, which are difficult to navigate, mine, and analyze effectively. We present sonification, the process of converting an oscillatory time series into audible sound, and citizen science, where members of the public contribute to scientific investigations, as a means to potentially help tackle these issues. Magnetometer data in the ULF range at geostationary orbit have been sonified and released to London high schools as part of exploratory projects. While this approach reduces the overall likelihood of useful results from any particular group of citizen scientists compared to typical citizen science projects, it promotes independent learning and problem solving by all participants and can result in a small number of unexpected research outcomes. We present one such example, a case study identified by a group of students of decreasing-frequency poloidal field line resonances over multiple days found to occur during the recovery phase of a coronal mass ejection-driven geomagnetic storm. Simultaneous plasma density measurements show that the decreasing frequencies were due to the refilling of the plasmasphere following the storm. The waves were likely generated by internal plasma processes. Further exploration of the audio revealed many similar events following other major storms; thus, they are much more common than previously thought. We therefore highlight the potential of sonification and exploratory citizen science in addressing some of the challenges facing ULF wave research.

**Plain Language Summary** Earth's magnetic shield, protecting us against harmful radiation from the Sun and more distant sources, is rife with a symphony of ultralow-frequency analogues to sound waves. These waves transfer energy from outside this shield to regions inside it and therefore play a key role in space weather. While they are too low pitch for us to hear them, we can make our satellite recordings of them audible by dramatically speeding up their playback. We show the audio can be used by school students to contribute to research, by having them explore through the act of listening and performing analysis using audio software. An example of this is presented where London school students identified waves whose pitch decreased over the course of several days. The waves were the natural oscillations of magnetic field lines, like the vibrations of a plucked guitar string, which forms a distinct note. The changing pitch is explained by the fact that the event occurred as Earth's magnetic shield was recovering from a disturbance caused by a *solar storm*. Many similar events were discovered in the audio, which also followed such disturbances, revealing that these types of waves are much more common than previously thought. Therefore, we have demonstrated that making data audible and involving the public can further the research into space weather.

## 1. Introduction

Ultralow-frequency (ULF) magnetohydrodynamic waves, with periods between seconds and tens of minutes, transfer mass, energy, and momentum throughout the solar wind-magnetosphere-ionosphere system. They can accelerate auroral and radiation belt electrons via wave-particle interactions and resonances (Chaston, 2013; Elkington, 2013) and routinely make significant contributions to local (and in extreme cases global) Joule heating of the ionosphere/thermosphere (Hartering et al., 2015). Many different modes of ULF waves may be excited within Earth's magnetosphere, driven by a variety of both internal and external processes, whose properties contain information about the processes that generated them and the regions through which they have propagated, resulting in a *zoo* of different ULF wave phenomena (McPherron, 2005; Wright & Mann, 2006). One example mode is the field line resonance (FLR), standing Alfvén waves on field lines approximately fixed at conjugate ionospheres (Southwood, 1974). It is known that FLRs' occurrence and properties (such as frequency) can be a highly variable depending on the solar wind and magnetospheric driving conditions present (e.g., Archer et al., 2017, 2015; Takahashi et al., 2010, 2014). However, historically, ULF waves in general have merely been classified as either quasi-sinusoidal or irregular and split into frequency bands, where the limits of these bands are not precise and more than one process may produce waves in a particular band (or across multiple bands; McPherron, 2005). Statistical studies often only consider how the integrated power over one or many of these bands varies with conditions (e.g., Mann et al., 2004); hence, narrowband or multiharmonic oscillations are not distinguished from broadband features in such studies. In cases where the former are considered, the methods used are often manual or semimanual (e.g., Takahashi et al., 2015). Given the vast amount of ULF wave data being produced by both space- and ground-based instruments, new techniques could potentially help.

Sonification is the use of nonspeech audio to convey information or perceptualize data (Kramer, 1994). Using the human auditory system has several advantages in temporal, spatial, amplitude, and frequency resolution over visualization techniques. For example, the human hearing range of 20–20,000 Hz spans 3 orders of magnitude in frequency and at least 13 orders of magnitude in sound pressure level (Robinson & Dadson, 1956), whereas the human visual system's perceptible frequencies range over only a quarter of an order of magnitude and no more than 4 orders of magnitude in luminance (Kunkel & Reinhard, 2010). Human hearing is highly nonlinear and has been shown to identify the pitch and timing of sound signals much more precisely than allowed by the Gabor limit or uncertainty principle (Oppenheim & Magnasco, 2013), which is a consequence of linear analysis methods such as the Fourier or wavelet transforms. While nonlinear analysis methods exist such as the Wigner-Ville distribution (Ville, 1948; Wigner, 1932) or empirical mode decomposition (Huang et al., 1998), these often introduce artifacts and mode mixing or can be unstable. Applications to magnetospheric ULF waves have shown that linear and nonlinear methods all have their own advantages and drawbacks depending on the precise nature of the waves present (Chi & Russell, 2008; Piersanti et al., 2018). Furthermore, the human auditory system's ability to separate sounds corresponding to different sources far outperforms even some of the most sophisticated blind source separation algorithms developed to date (Divenyi, 2005). Therefore, it is clear that there should also be a place for data sonification in addition to both standard and more recent methods of analysis.

There is a long history of converting space plasma physics data into audible sounds; for example, the terminologies of ionospheric extremely low frequency (ELF) and very low frequency (VLF) waves, which largely span the human hearing range, such as *whistlers* (Barkhausen, 1919) and *lion roars* (Smith et al., 1967) were based on their psychoacoustics when picked up by radio antenna. This tradition has continued with nomenclature such as *tweaks*, *chorus*, *hiss*, and *static* being commonly used in magnetospheric and ionospheric ELF/VLF research, and various ELF/VLF data sets from across the solar system are available in audio format (e.g., <http://space-audio.org/>).

Sonification techniques can also be used for waves normally outside of the human auditory range. Depending on the time resolution of the data and the frequency ranges of interest, sonification can dramatically cut down on the analysis processing time, making it ideal for effective navigation, mining, and analysis of *big data* within exploratory research (Hermann, 2002). Alexander et al. (2011, 2014) and Wicks et al. (2016) showed that researchers using sonified solar wind data were able to identify subtle features embedded within the data that were not necessarily clear from standard visual analysis techniques. However, sonification of magnetospheric ULF wave data sets is not widespread. The only publicly available example we are aware of is the Canadian Array for Realtime Investigations of Magnetic Activity (CARISMA) ground magnetometer network's

induction coil magnetometer data (<http://www.carisma.ca/>). Each day of 20-Hz resolution data is filtered and resampled as 44,100-Hz audio, allowing waves of frequencies down to 9 mHz in theory (though in practice the lower limit will likely be higher depending on the subject) to be heard. However, this entirely neglects the Pc5 band of ULF waves (2–7 mHz) and some of the Pc4 band also (7–22 mHz), both of which play important roles within the magnetosphere.

Another fairly recent technique to tackle large data sets is that of citizen science, involving “organized research in which members of the public engage in the processes of scientific investigations by asking questions, collecting data, and/or interpreting results” (CitizenScience.org). It typically works by the concept of crowdsourcing and can collect data and/or analysis, which may be extremely difficult and/or inefficient to be carried out either by a small number of researchers or by using computational algorithms. This crowdsourcing model therefore requires well thought-out, highly prescribed activities to be undertaken by all the citizen scientists. It should also be noted that as well as the benefits to the research, citizen science should also positively impact upon the volunteers who participate through their educational and outreach/engagement elements. While formalized citizen science projects are well established in areas such as astronomy and biology, they are rare in space plasma physics (Knipp, 2015). Solar Stormwatch, integrated into the Zooniverse.org platform, uses citizen scientists to track the propagation of coronal mass ejections (CMEs) through the heliosphere (Barnard et al., 2014). Sunspotter (<http://www.sunspotter.org>) tasked citizen scientists to rank images of sunspots by their complexity. Aurorasaurus maps the location of the auroral oval by taking advantage of geotagged posts on Twitter, which are verified by citizen scientists as having been auroral observations (MacDonald et al., 2015). Clearly, there is scope to do more in this area within the field.

This paper presents a project that uses sonification to enable exploratory citizen science research into magnetospheric ULF waves called Magnetospheric Undulations Sonified Incorporating Citizen Scientists (MUSICS, <http://www.qmul.ac.uk/spa/musics>). Magnetometer data at geostationary orbit were made audible in the ULF range and given to high school students as part of independent projects. We present the sonification process, framework of the exploratory citizen science, and first results emerging from the MUSICS project.

## 2. MUSICS Project

### 2.1. Sonification

While many different forms of sonification are possible, we use the simplest method, which is sometimes known as audification. This is the direct translation of time series data to audio samples, hence is only applicable to an already oscillating signal and thus clearly relevant to the study of magnetospheric ULF waves. The sonified data can then be analyzed by the human auditory system, rather than the forms of visual analysis usually performed. Alexander et al. (2014) provide a detailed list of considerations when attempting this process; here we detail the methods chosen for use in ULF wave sonification applied to Geostationary Environment Operational Satellite (GOES) data.

The sonification was applied to each year of GOES magnetometer data at 512-ms resolution. Currently, these data are available for 2007–2008 (GOES-10, GOES-11, and GOES-12) and 2010–2017 (GOES-13 and GOES-15). Before sonification, the ULF waves must first be extracted from the data and transformed into an appropriate coordinate system—a fairly standard procedure. The original data in PEN coordinates were used, where P is perpendicular to the satellite’s orbital plane, E lies parallel to the satellite–Earth center line and points earthward, and N is perpendicular to both pointing eastwards. A mean-field-aligned coordinate system was defined by taking a 34-min running average of the data, whose direction at each time shall henceforth be called the compressional component (com) since magnetic field oscillations in this direction are representative of compressional modes. The two remaining directions defining the coordinate system are the poloidal component (pol), corresponding to the direction perpendicular to the mean field pointing radially outward from the Earth, and the toroidal component (tor), perpendicular to both and directed azimuthally toward east. The data were transformed into this coordinate system, and the running average was subtracted from the compressional component, thereby extracting ULF waves of frequencies  $\gtrsim 0.5$  mHz. Any data gaps were interpolated for the coordinate transformation and subsequently filled with zeros to ensure a full year of regularly sampled data for the sonification.

The choice of a lowest-frequency scale of 0.5 mHz was made for numerous reasons. The first concerns known and/or theorized ULF wave modes. The magnetospheric density survey of Archer et al. (2015) showed that the lowest expected fundamental frequencies of FLRs at geostationary orbit in the dawn, noon, and dusk sectors

across half a solar cycle were all around 0.7 mHz. Furthermore, the proposed eigenmode of the dayside magnetopause is also expected to typically have similarly low frequencies, with these being less than 0.5 mHz only 10% of the time (Archer & Plaschke, 2015). The second reason for the choice of scale pertains to spacecraft motion. Over 34 min the GOES spacecraft's azimuthal position changes by about 8°; however, over much longer time scales the spacecraft motion can no longer be neglected and one risks mixing spatial and temporal effects (Urban et al., 2016). Furthermore, when considering such long timescales the mean field no longer becomes representative of the background geomagnetic field, rendering the field-aligned coordinate system inadequate at distinguishing between the physical processes behind the ULF waves.

For effective conversion to audio, it is necessary to tailor the sampling rate of the output such that frequencies of interest will map to the human auditory range of approximately 20–20,000 Hz. The relationship between the real frequency of a signal in the data  $f_{\text{real}}$  to that in the audio  $f_{\text{audio}}$  is given by

$$f_{\text{audio}} = f_{\text{real}} \times F_s \Delta t_{\text{real}}, \quad (1)$$

where  $\Delta t_{\text{real}}$  is the cadence of the original data and  $F_s$  the sampling frequency of the outputted audio. A widespread standard sampling frequency in audio is  $F_s = 44,100$  Hz since this corresponds to a Nyquist frequency just above the upper threshold for humans. However, this simple mapping would render the lowest frequencies present in the data inaudible. The data were therefore boxcar averaged by four data points, down-sampling its resolution to  $\Delta t_{\text{real}} = 2.048$  s before the conversion. The sonification, therefore, has made the vast majority of all physically meaningful frequencies in the GOES data audible.

Two different types of audio were produced: a straightforward conversion of the magnetic field data and a spectrally whitened data set produced by first time-differencing the data (e.g., Takahashi et al., 2010) and then sonifying. Since audio waveforms are unitless and must lie within the range  $-1$  to  $1$ , some form of amplitude scaling must also be performed. In order to preserve the natural variability of the data, we simply scale the data by dividing through by factors of 10 nT and 0.49 nT/s, respectively—less than typical ULF wave amplitudes (e.g., Takahashi et al., 2012). Any values greater than these thresholds were clipped to the maximum waveform values of 1 or  $-1$ . Clipping occurred less than 3% of the time.

While each component was output separately as a mono audio file, a summary stereo file was also produced, corresponding to the poloidal component in the left channel, the toroidal component in the right channel, and the compressional channel multiplied by a factor of 0.5 added to both channels. This enables one to listen to all three components at once and perform a cursory polarization analysis (particularly when using headphones) by judging whether any identified events are loudest in either the left or right ears or approximately of equal loudness in both ears.

Through this sonification process each year of data is converted into approximately 6 min of audio. The time within the audio is given by

$$t_{\text{audio}} = \frac{t_{\text{real}}}{F_s \Delta t_{\text{real}}}, \quad (2)$$

assuming that the actual time  $t_{\text{real}}$  starts at zero at the beginning of each year. Ogg Vorbis compression was used to write the audio files since this does not suffer the issues of MP3 encoders, which introduce silence at the beginning of audio files thereby rendering the time conversions in equation (2) incorrect. Given the longitudes of the GOES spacecrafts' geostationary orbits, local time can also be easily calculated. Therefore, the sonification dramatically reduces the time frame of the data, allowing for fast surveying of ULF wave big data with the ability to ascertain the real times and locations of events.

## 2.2. Citizen Science

While sonified data have been used as a tool for researchers, we are not aware of its widespread use in exploratory citizen science projects. However, given the ease of data navigation, mining, and analysis afforded, we believed it would lend itself well to such efforts by lowering the barrier to entry of getting involved. Furthermore, since everyone's perception of sound is different and pattern recognition (particularly of weak or noisy signals) within audio improves with practice (Whitton et al., 2014), utilizing a wide pool of citizen scientists listening to the same data set should identify numerous different types of events, whereas use of sonified data by a single researcher might only highlight just one or a few. Therefore, a project was developed for London schools as part of a wider initiative enabling high school students to experience research science and independently develop their own investigations. The main aim of this initiative is on raising students' aspirations toward physics (or STEM), with potential benefits toward the research being of secondary concern. This

is somewhat different to most citizen science, where addressing the scientific objectives is of primary importance. To highlight this difference in aim as well as the educational environment in which they are set, such initiatives are sometimes called *Research in Schools* rather than citizen science despite the similarities between the two approaches. Details on the first couple of years of the entire Research in Schools program, preliminary results on the impact it has had on students and teachers, and the lessons learned about setting up such a program can be found in Archer (2017). To summarize, students report having increased their confidence in various topics and scientific methods related to their project area to a high level of statistical significance (currently the MUSICS project has an overall 6.1 z score in a Wilcoxon signed-rank test; Wilcoxon, 1945), as well as developing a wide array of different skills many of which they would likely not have had access to previously in their school environment. Teachers fed back having learnt new physics content and developed skills, which could be implemented or referred to in future lessons, as well as gaining confidence in supporting their students and discussing research content with them.

The MUSICS project runs for 6 months each year from around the start of the U.K. autumn term and ending before the easter/spring break, after which the students involved (ranging from 14- to 18-year-olds) typically have exams. At the start of the project the students are introduced to the area of magnetospheric ULF wave research and are given a written introductory guide, the sonified data, free Audacity audio software (<http://www.audacityteam.org/>), and a standard spreadsheet for logging events. The audio software allows the students to perform several standard analysis methods simply within the graphical user interface including plotting power spectra, spectrograms, correlation-based pitch analysis, and root-mean-square amplitude computations, with an example view shown in Figure 1. Indeed, much of the analyses presented in section 3 are possible within the software, requiring no programming expertise by the students. The spreadsheet provided implements conversions of time, local time, frequency, and amplitude applied to the sonified data. Students are encouraged to first explore the data and the tools provided before in small groups focusing on investigating a single or class of similar events that they have identified aurally. Throughout the project they are supported both by their teacher and a number of visits from researchers, providing suggestions of how they can progress with their project as well as the wider context of what they have done in terms of previous research. At the end of the project they, along with students working on other projects within the wider program, present their work either as a talk or poster at a special student conference.

Such an exploratory model of citizen science has its benefits and drawbacks. Most citizen science is highly prescriptive to the participants, since they are presented with one or a series of carefully constructed questions or tasks to follow. In this respect the citizen scientists are largely being used to crowdsource data/analysis, which may be difficult to implement by individuals or algorithmically. Therefore, the focus is on producing a usable data set rather than on the independent learning and problem solving of the participants. Such a model has its benefits as the aggregated citizen science data may easily be implemented in tackling the intended research. Because of this, however, these projects primarily address one or a limited number of science questions. While there is sometimes scope for unexpected results, typically through citizen scientists discussing and collaborating with researchers on discussion boards, such activities are undertaken by a very small minority of citizen scientists. In contrast, the Research in Schools style of projects, such as MUSICS, provide much less prescription than standard citizen science because the focus is on independent learning and problem solving by the participants, an important aspect of a researcher's experience that typical citizen science tends to emphasize less, in order to positively impact upon the students involved. All citizen scientists in this model are encouraged to tailor or adapt their methods depending on what they have discovered, through collaboration with researchers. This is the primary methodology used for all involved, rather than something undertaken by only a fraction of participants. Of course, the overall likelihood of useful results from any particular group of citizen scientists toward the research is reduced in this case compared to typical citizen science. Nonetheless, in the next section we show that this model of citizen science can indeed result in unexpected research outcomes. We therefore stress that both models of citizen science have their merits.

### 3. First Results

To demonstrate the potential of using sonified ULF wave data in citizen science projects for original research, the first results from the MUSICS project are presented. Students at Eltham Hill School in South East London aurally identified a case study event from the sonified GOES magnetometer data. Based on the students' initial work, here we present the results of more detailed research performed by professional scientists into that



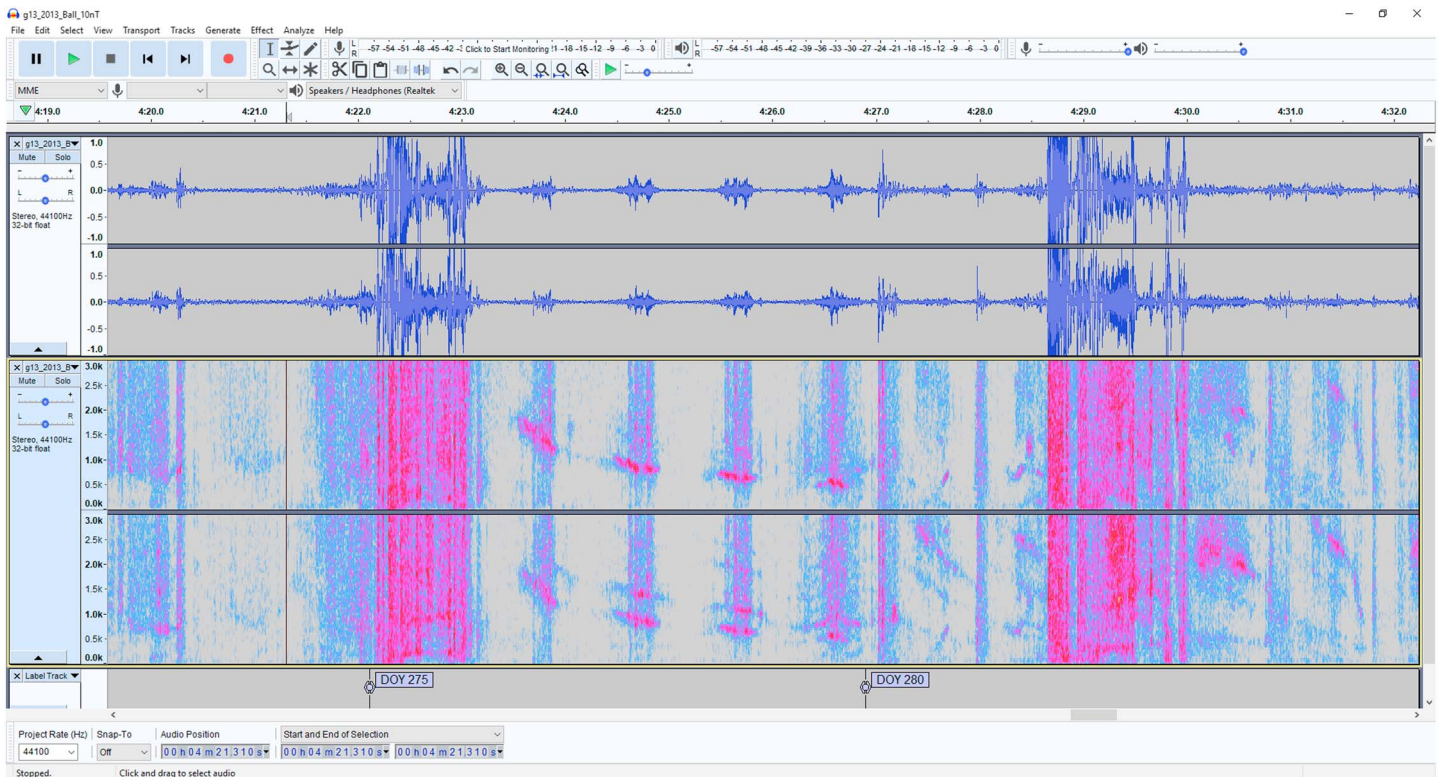


**Figure 1.** Citizen scientists' view in Audacity of the event presented in section 3. The top tracks show the waveform view of the GOES-13 summary stereo audio file whereas the bottom tracks show the spectrogram view of the GOES-13 time-differenced summary stereo audio file. Labels have been added in the software to denote day-of-year ranges. DOY = day of year; GOES = Geostationary Environment Operational Satellite.

event. Thus, the scientific results presented in this paper were made possible only thanks to the citizen scientists' identification of the event and their preliminary analysis of it. Note that the analysis here uses the GOES magnetometer data in the mean-field-aligned coordinate system but before its conversion into audio, so no issues arise due to, for example, clipping of waveforms.

### 3.1. ULF Wave Observations

The case study event occurred between 2 and 6 October 2013 (days of year 275–279). Figure 2 shows both the time series of each component of the magnetic field and their corresponding spectrograms (using 1,024-sample Hanning windows of the time-differenced data with 50% overlap). Compare this with the Audacity view of the same event in Figure 1 as well as the equivalent audio, which can be found in the supporting information. The event consisted of large-amplitude broadband waves lasting a day, followed by intervals of narrowband near-sinusoidal waves over the following four days. The corresponding local times of these intervals, initially identified by the citizen scientists through their use of the provided spreadsheet, stayed relatively constant throughout at ~07–17 hr; thus, their duration each day in the data is a spatial and not temporal effect with both spacecraft encountering the waves each day/orbit. Oscillations were predominantly in the poloidal component (a feature noted by the citizen scientists), which had 50% of the total power overall, followed by the toroidal (28%) and compressional (22%) components. These percentages varied by  $\pm 15\%$  when investigating subintervals.

It is apparent from the spectrograms that the frequencies of the narrowband waves decreased throughout the event, spanning the Pc3–5 frequency bands. It should be noted that this feature was what initially alerted the citizen scientists to the event, as it was far more striking through listening to the audio than cursorily glancing at spectrograms alone. Therefore, the event was discovered thanks to the combined sonification and exploratory citizen science elements of MUSICS. The citizen scientists performed an initial characterization of the frequency decrease with time by using Audacity's spectral tools (e.g., see spectrogram in Figure 1), converting frequencies from the audio to their physical values in the provided spreadsheet. Here we perform a more thorough frequency-time analysis. Because of the large variance associated with the spectrogram's

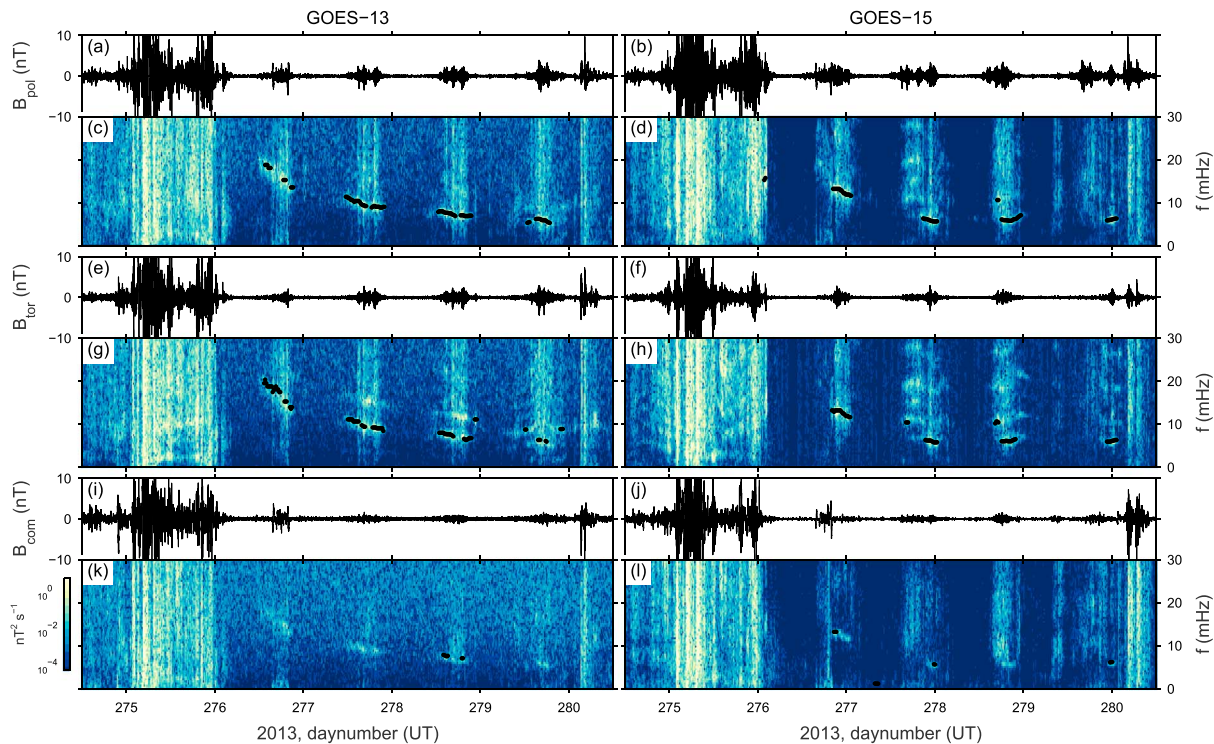


**Figure 2.** GOES-13 (left column) and GOES-15 (right column) magnetometer observations of a long-lasting ultralow-frequency wave event displaying time series of the (a, b) radial/poloidal, (e, f) azimuthal/toroidal, and (i, j) field-aligned/compressional components along with their respective whitened spectrograms (c, d; g, h; and k, l). Black dots indicate identified frequencies using an autocorrelation-based method. GOES = Geostationary Environment Operational Satellite.

spectral estimators, we opt to quantify the frequencies using an autocorrelation method based on Tolonen (2000), widely used in audio analysis and described in Appendix A.1. The corresponding frequencies are indicated in Figure 2 as the black dots, which overall show good agreement with the lowest harmonics of the narrowband waves in the spectrograms. There are a few windows at the beginning or end of some days' observed waves where a higher harmonic seems to have been selected due to little power at lower frequencies. These instances have been manually removed in further analysis.

To ascertain the polarization properties of the waves, the spectral matrix of each 1,024-sample window of differenced data was calculated for all magnetic field component pairs using Welch's overlapped averaged periodogram method with eight segments (see Appendix A.2). The cross-phase between the poloidal and toroidal components ( $\phi_{\text{pol}} - \phi_{\text{tor}}$ ) is shown in Figures 3a and 3b as the hue, revealing they were largely close to antiphase with one another though with considerable variability. To better quantify this, the average phase difference, weighted by both cross-power and coherence, and its spread were calculated. These were  $\phi_{\text{pol}} - \phi_{\text{tor}} = -173 \pm 52^\circ$ ,  $\phi_{\text{pol}} - \phi_{\text{com}} = -16 \pm 55^\circ$ , and  $\phi_{\text{tor}} - \phi_{\text{com}} = -179 \pm 45^\circ$ . The parameters of the polarization ellipse in the transverse plane were also calculated (Arthur et al., 1976), namely, the orientation  $\psi$  and ellipticity  $\chi$  angles whose definitions are depicted in Figure 3g. The ellipse's orientation (Figures 3c and 3d) shows no systematic change with local time across the four wave intervals with a weighted average value and spread of  $\psi = 42 \pm 30^\circ$ . Similarly, there is little change in the ellipticity angle (Figures 3e and 3f), and its value is very low, that is, close to plane polarization, at  $\chi = 3 \pm 12^\circ$ . The average polarization ellipse of the event is depicted in Figure 3g.

Similar cross-phase analysis was performed between the two GOES spacecraft (not shown) in order to estimate the waves' azimuthal wave numbers  $m$ . However, the coherence was found to be poor ( $<0.3$ ) throughout, and thus, a reliable cross-phase could not be determined. Given the azimuthal separation of the two spacecraft of  $60^\circ$ , corresponding to a maximum determinable  $m$  of 6, such low coherence may indicate higher wave numbers.

It should be noted that a search for ground magnetometer signatures of this event throughout the International Monitor for Auroral Geomagnetic Effects (IMAGE) network yielded no waves matching the frequencies

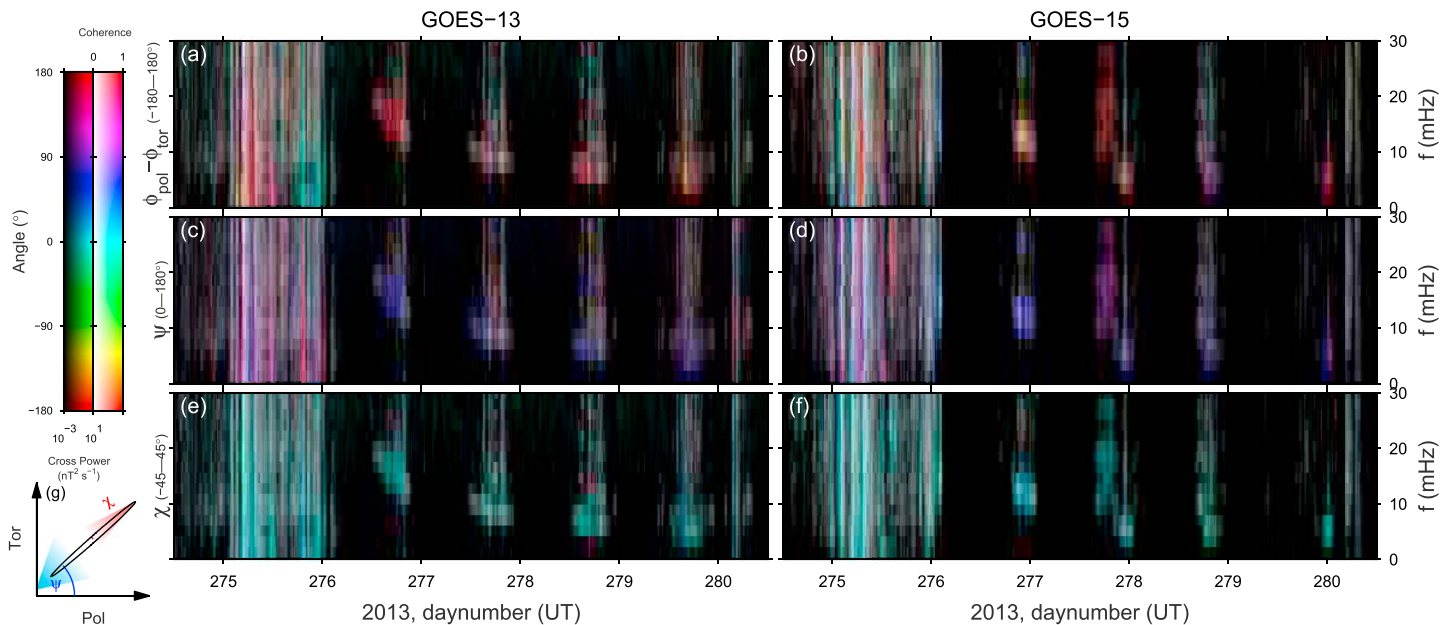


**Figure 3.** Polarization parameters displayed using the HSV color model depicting angles (hue), coherence (saturation), and cross-power (value). Panels correspond to (a, b) the phase difference between poloidal and toroidal components, (c, d) the orientation angle of the polarization ellipse, and (e, f) the ellipticity angle. The latter two angles are depicted in panel (g) along with the average polarization ellipse (black) and angular spreads (colored areas). GOES = Geostationary Environment Operational Satellite.

observed by GOES. This may also point toward high  $m$  waves since these get screened by the ionosphere, making them difficult to detect on the ground (Hughes & Southwood, 1976).

### 3.2. Analysis

The citizen scientists looked into solar wind observations throughout the event, taken from the OMNI database, revealing a CME as shown in Figure 4. The start of the initial broadband wave activity corresponded with the arrival of the CME shock, indicated by the sharp increase in the solar wind density and speed (Figures 4b and 4c, respectively) as well as interplanetary magnetic field (IMF) strength (Figure 4a), with these waves lasting for the duration of the CME's subsequent sheath region. The large increase in the solar wind dynamic pressure associated with the CME would have moved the magnetopause standoff distance to within geostationary orbit based on the Shue et al. (1998) model. However, from the positions of the two GOES spacecrafts with time, they should not have encountered the magnetopause. Indeed, there was no indication from the original magnetometer data of any magnetopause crossings.

Following the CME sheath was a magnetic cloud, a region of low density and elevated IMF strength (compared to background values) along with slow rotations in IMF orientation. The narrowband waves, which were first very briefly observed by GOES-15 at the start of day 276, seemed to commence around the time of the arrival of the magnetic cloud, though the waves lasted beyond the cloud's duration. We note that while the start of these waves could clearly be heard in the audio and was identified by the autocorrelation algorithm (see Figure 2d), this was not clear at all from looking at the time series or spectrogram. To check for the possibility that the waves were directly driven by the solar wind, we looked at 3-s resolution plasma and magnetic field data from the ARTEMIS spacecraft in lunar orbit (Angelopoulos, 2010; Auster et al., 2008; McFadden, Carlson, Larson, et al., 2008) but found no similar oscillations present.

The CME's arrival at the magnetosphere triggered a geomagnetic storm, as indicated by the  $Dst$  and  $Kp$  activity indices (Figures 4d and 4e), which was the largest of 2013 as measured by  $Kp$  and the tenth largest by  $Dst$ . The occurrence of the narrowband waves coincided with the recovery phase of the storm.

During the event the Time History of Events and Macroscale Interactions during Substorms (THEMIS; Angelopoulos, 2008) spacecraft had apogees in the dusk sector, with their outbound trajectories crossing geostationary orbit at around 19 hr local time. This unfortunately meant that they did not observe the narrowband ULF waves and their radial extent. Using spacecraft potential inferred density measurements (Bonnell et al., 2008; McFadden, Carlson, Bonnell, et al., 2008) from outbound crossings of THD and THE, we extended



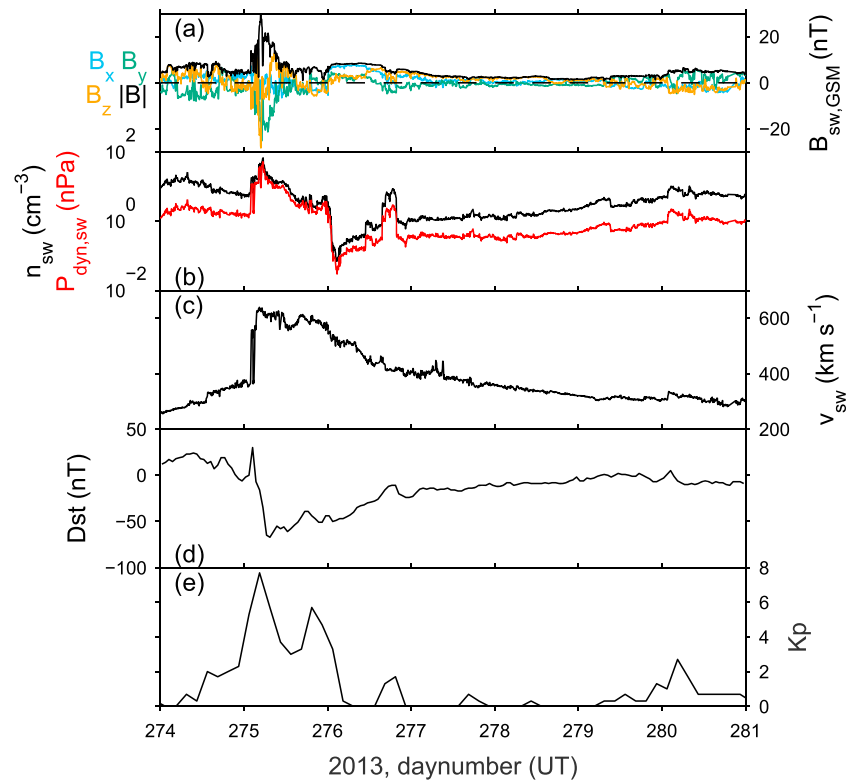


**Figure 4.** Solar wind and geomagnetic conditions showing (a) the interplanetary magnetic field strength (black) and geocentric solar magnetospheric components ( $x$ ,  $y$ , and  $z$  as blue, green, and orange, respectively), (b) solar wind density (black) and dynamic pressure (red), (c) solar wind speed, and the (d)  $Dst$  and (e)  $Kp$  geomagnetic activity indices.

the electron density radial profile survey of Archer et al. (2015). The evolution of these profiles is depicted in Figure 5a. This reveals an extended plasmasphere before the event, with the CME and resulting storm causing the erosion of magnetospheric plasma and recession of the plasmapause. Refilling of magnetospheric plasma occurred throughout the time of the narrowband waves. This is shown more clearly for the electron density measurements at geostationary orbit displayed in Figure 5b. The apparent refilling rate approximately followed a two-step process with exponential growth rates of

$$\frac{d \log_{10}(n_e)}{dt} = \begin{matrix} 0.77 \pm 0.05 \text{ day}^{-1} & \text{Early} \\ 0.46 \pm 0.07 \text{ day}^{-1} & \text{Late} \end{matrix} \quad (3)$$

corresponding to  $\sim 1 - 10 \text{ cm}^{-3} \text{ day}^{-1}$  initially, followed by  $\sim 13 - 33 \text{ cm}^{-3} \text{ day}^{-1}$ . These are consistent with previously reported observations (Lawrence et al., 1999). It is natural to think that the narrowband waves were FLRs whose decreasing frequency was a result of the increasing magnetospheric density and thus decreasing Alfvén speed.

The average frequency of poloidal FLRs at geostationary orbit across the dayside was estimated by solving the Singer et al. (1981) equation applied to a T96 magnetic field model (Tsyganenko, 1995, 1996), using the median conditions over the event combined with the THEMIS density observations. An average ion mass of 7.5 amu (Sandhu et al., 2016) was used along with the usual power law form for the density along the field lines using exponent  $\alpha = 1$  (Denton et al., 2015). Changing the fixed parameters within their respective interquartile ranges affected results by less than 10%. The estimated second and fourth harmonics are shown in Figure 5c, since even modes should be most prominent in magnetic field data close to the magnetic equator. While local time differences at geostationary orbit from T96 alone are negligible, these calculations assume that the density measured near dusk is representative of all dayside local times, which is not true in general. However, Figure 5c also shows the identified frequencies of the waves from both spacecraft colored by local time, revealing several instances of similar frequencies observed simultaneously at different local times and a near continuity of frequencies with time. This suggests a global expansion of the plasmasphere throughout

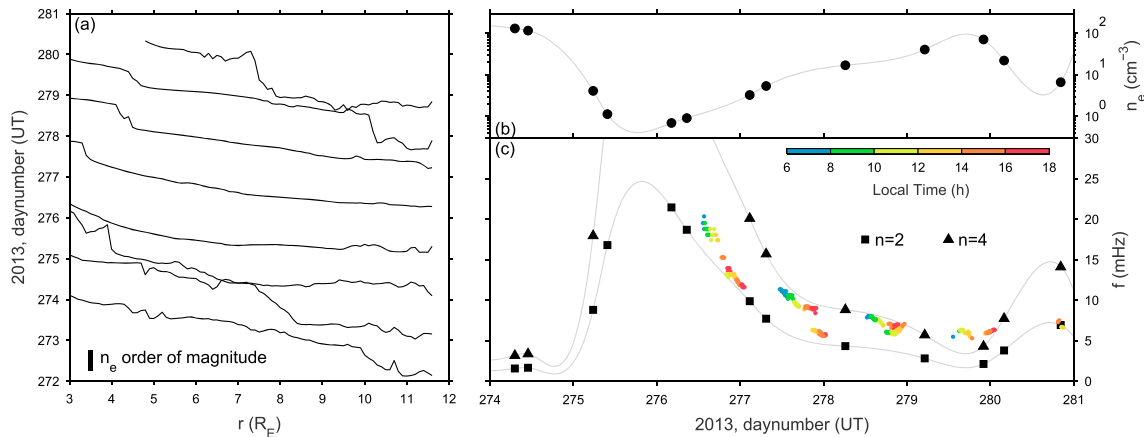


**Figure 5.** (a) Time History of Events and Macroscale Interactions during Substorms magnetospheric radial plasma density profiles at 19 hr LT stacked by time, (b) plasma density at geostationary orbit, and (c) estimated frequencies of even mode poloidal field line resonances based on the density observations. The observed frequencies are overlaid and colored by local time.

the event. There is good agreement between the estimated frequencies and those observed by GOES; thus, the refilling can explain the decreasing frequency of the observed waves across the event. Interestingly, as the event progresses there appears to be a change in the FLR harmonic as the frequency drops, seemingly going from predominantly the second to later the fourth harmonic.

It is known that field line resonant frequencies at geostationary orbit exhibit dependence on solar wind and geomagnetic conditions (e.g., Takahashi et al., 2010). Hourly averages of the observed frequency and conditions across this event were taken, with the correlation coefficients and their standard errors displayed in Table 1 (rank-order correlation coefficients were similar). This was also done for the second harmonic FLR frequency  $f_2$  where instances of what appears to be the fourth harmonic were corrected by the ratio of the second and fourth harmonics from our FLR frequency estimates. In most cases  $f_2$  shows ever so slightly higher levels of correlation. The correlation between estimated FLR frequencies with hourly averaged conditions from the Archer et al. (2015, 2017) survey across half a solar cycle is also shown in the dawn, noon, and dusk sectors for comparison, where the standard errors are less than  $\pm 0.03$ . As pointed out by the citizen scientists, for this event the frequency was highly correlated to the solar wind speed and IMF strength. The latter was predominantly due to the geocentric solar magnetospheric  $z$  component, despite the IMF being northward throughout the intervals of narrowband waves, with a fair level of correlation also due to the  $x$  component. These results may have been down to chance for this specific event, given there is little to no correlation between geostationary FLR frequencies and the IMF in general. While around noon and dusk it is known that there is some degree of correlation between the solar wind speed and geostationary FLR frequencies, the observed correlation for this event is much higher. Similar levels of correlation are typically expected for the  $Dst$  index though the correlation for this event, while fair, was not as strong. This highlights the potential importance of the storm phase and thus the time history of the magnetosphere, in density and FLR frequency models.

### 3.3. Discussion

First, we discuss the possible driving mechanisms of the observed narrowband waves in this event. We have already excluded the possibility that these waves were directly driven by the solar wind since similar

**Table 1**  
Correlation Coefficients of Hourly Averaged Frequencies With Solar Wind and Geomagnetic Conditions

| Frequency                   |      | $B_{sw}$        | $B_{x,sw}$      | $B_{y,sw}$       | $B_{z,sw}$      | $n_{sw}$        | $v_{sw}$        | $Dst$            | $AE$             |
|-----------------------------|------|-----------------|-----------------|------------------|-----------------|-----------------|-----------------|------------------|------------------|
| $f$                         |      | $0.92 \pm 0.03$ | $0.72 \pm 0.08$ | $-0.27 \pm 0.16$ | $0.80 \pm 0.06$ | $0.28 \pm 0.16$ | $0.92 \pm 0.03$ | $-0.71 \pm 0.09$ | $0.00 \pm 0.17$  |
| $f_2$                       |      | $0.96 \pm 0.01$ | $0.70 \pm 0.09$ | $-0.34 \pm 0.15$ | $0.84 \pm 0.05$ | $0.30 \pm 0.16$ | $0.94 \pm 0.02$ | $-0.70 \pm 0.09$ | $-0.23 \pm 0.16$ |
| (Archer et al., 2015, 2017) | Dawn | 0.04            | 0.02            | -0.07            | -0.06           | -0.1            | 0.24            | -0.17            | 0.14             |
|                             | Noon | 0.02            | -0.05           | -0.04            | 0.01            | -0.21           | 0.54            | -0.41            | 0.17             |
|                             | Dusk | 0.17            | -0.01           | 0.01             | -0.06           | -0.20           | 0.52            | -0.54            | 0.17             |

oscillations were not present upstream in particle or magnetic field measurements. However, significant changes in the solar wind dynamic pressure were present throughout, and perhaps these could have resonantly excited the observed FLRs. It is expected that waves generated by this mechanism are toroidally polarized and have low  $m$  (Allan et al., 1986; Mann et al., 1998; Southwood, 1974; Tamao, 1965), unlike the observed event. Similarly, Alfvén waves excited via the Kelvin-Helmholtz instability would be expected to also have low  $m$  and to exhibit a reversal in polarization about noon due to the change in the flow direction within the magnetosheath around the subsolar point (Agapitov et al., 2009; Dungey & Southwood, 1970; Samson et al., 1971); however, no such reversal was seen. Indeed, high  $m$  waves, as we suppose is the case for this event, are a signature of internally and not externally driven waves (Le et al., 2017; Southwood et al., 1969). Furthermore, the even harmonic field line resonances observed imply an energy source that acts asymmetrically about the equator, whereas externally driven waves tend to be more often symmetric about this plane.

Therefore, we conclude that the processes generating the narrowband waves likely were internal to the magnetosphere. Based on typical periodicities, energy may be transferred to waves via drift and/or bounce resonances with radiation belt electrons, ring current ions, or the background ion population. It has been suggested that observed poloidal waves may be excited by bounce resonance with energetic (predominantly  $H^+$ ) ions and that these are likely second harmonic FLRs (Glassmeier et al., 1999; Hughes et al., 1978; Southwood et al., 1969). Ferradas et al. (2018) showed using Van Allen Probes observations that this particular geomagnetic storm injected ions at energies above  $\sim 10$  keV. This therefore demonstrates that there was free energy available for conversion to wave power. We calculate the pitch angle-averaged minimum bounce frequencies of these ions based on their lower energies to be approximately 2 mHz ( $O^+$ ), 4 mHz ( $He^+$ ), and 8 mHz ( $H^+$ ). These values can potentially explain the change in harmonic throughout the event. While the eigenfrequencies of the field lines were decreasing throughout the event due to the plasmasphere refilling, the bounce frequencies are unaffected by this. Therefore, as the frequency of the second harmonic dropped to around the lowest possible bounce frequency, the ion bounce resonance became more effective at driving fourth harmonic waves. This hypothesis, coupled with the lack of change in polarization from poloidal to toroidal mode Alfvén waves, suggests that continuous driving occurred throughout the event.

This event shares some characteristics of a type of ULF wave known as giant pulsations: highly monochromatic poloidal oscillations in the Pc4 (7–22 mHz) band that are localized in latitude, have large azimuthal wave numbers, and can continue for two or more days (e.g., Green, 1985; Rostoker et al., 1979). They are thought to be caused by protons with energies of 5–30 keV drifting from the nightside. However, giant pulsations are fundamental mode FLRs observed on the ground concentrated in the dawn sector (though they have recently been shown to also occur at dusk; Motoba et al., 2015), which occur during quiet or late storm recovery periods and most often at solar minimum. These properties are all unlike this event; therefore, it cannot be deemed to be a giant pulsation.

Other long-duration Pc5 waves have been published though these share little similarities with this event since they tend to be predominantly compressional waves in the nighttime sector during the start of storm times (Takahashi et al., 1985; Takahashi, Fennell, et al., 1987; Takahashi, Lopez, et al., 1987). To our knowledge only two truly similar events to this have been previously reported. Sarris, Li, and Singer (2009) presented an apparently rare narrowband Pc5 event in GOES magnetometer data from 1997 lasting 5 days during the recovery phase of a storm. The waves were chiefly poloidally oriented (though packets of phase mixing from poloidal to toroidal mode were observed within the event; Sarris, Wright, & Li, 2009) with frequencies decreasing with time from 9 to 5 mHz over the course of the event. Density measurements from the LANL spacecraft, also in geostationary orbit, revealed local evidence of a plasmasphere refilling process associated with the observed slow frequency decrease. The waves' azimuthal extent shrank throughout the course of the event, initially spanning some 12 hr across the dayside and by the end of the event being concentrated over 7 hr of local time in the noon and postnoon sectors. This feature is unlike our observations, where the azimuthal extent remained widespread and almost constant throughout. Also, unlike the event presented here, Sarris, Li, and Singer (2009) found signatures of the waves in ground magnetometer data revealing large  $m$  values between 20 and 55 and an eastward propagation in all local time sectors. They also concluded that these waves were likely driven by internal particle anisotropies and not via external mechanisms. Korotova et al. (2016) reported a Pc4 event observed by Van Allen Probes, THEMIS, and GOES over 1.5 days during the late recovery phase of a moderate storm in 2014. These were observed throughout most of the morning sector except for by GOES, which only observed the waves in the late afternoon sector, unlike the event presented here. They showed that these were even harmonic (likely the second harmonic based on previously

reported frequencies) poloidal FLRs and that they spanned a number of L-shells, dissimilar to the Sarris, Li, and Singer (2009) and Sarris, Wright, and Li (2009) event. The frequencies of these waves decreased over the course of successive orbits from 17 to 12 mHz based on the GOES observations and down to ~8 mHz at geostationary L-shells based on the other spacecraft measurements, with some evidence of plasmasphere refilling occurring. Again, they attributed the source of the pulsations as due to proton bounce resonance. Similar events to the case study are therefore little discussed in the literature and indeed thought to be rare. The MUSICS project was thus not designed with this class of event in mind; nonetheless, the combination of sonification and exploratory citizen science uncovered one such example.

To better put this event into context and to test whether such events are indeed rare, we navigated the sonified GOES-13 poloidal component data searching for similar events, thereby taking advantage of the reduced time frame of the sonified data. More precisely, this search looked for decreasing-frequency narrowband waves spanning at least 1 day, revealing 21 events in 2013 alone. We note that many of these events were much more subtle, even in the sonified data, than the case study being often weaker and/or superposed with other waves. Only through the case study having been identified by the citizen scientists and through auditory training (listening to the event numerous times) was it possible to then pore through the audio to easily identify further events (cf. Whitton et al., 2014). The start of each event was identified as the beginning of the first interval (where each interval as per the case study is a fraction of a day in duration due to the limited local times of the waves) of the decreasing-frequency narrowband poloidal waves, with the duration of the event being the time until the end of the very last interval of narrowband waves, which continued the decreasing-frequency trend. No overlap in events occurred. Figure 6a shows the number of events in occurrence as a function of time from their start. The median duration was 3.0 days, and the longest event lasted 5.4 days, with the total duration of all events being 60.5 days, that is, 17% of the entire year. Therefore, such events cannot be considered rare.

A superposed epoch analysis of the solar wind and geomagnetic conditions for these 21 events was performed to ascertain the typical driving conditions, which are shown in Figures 6b–6g where the start of the ULF wave event was set as the zero epoch and the median and interquartile ranges (and their respective standard errors) were calculated at each epoch time. Of course, since the ULF wave events have a limited extent within local time, an ambiguity between temporal and spatial effects exists within this analysis. The result will be a smearing out of the superposed epoch analysis over timescales of at most 1 day. The clearest and most significant results are in the indices of geomagnetic activity revealing, like with the case study event, increased activity for a period of about a day immediately before the start of the wave events, indicative of storm conditions beforehand. All quartiles of the *Dst* index show slow returns to prestorm levels over the course of several days starting around the time of the events. Furthermore, there was a one-to-one correspondence between many of these events and geomagnetic storms listed at <http://www.spaceweatherlive.com>. Thus, such ULF wave events typically occur (at least initially) during the recovery phase of geomagnetic storms. It is not clear, however, whether all storms (meeting some criteria) result in these ULF wave events. Storms are obviously more common during solar maximum, which was the case for 2013, whereas the observations of Sarris, Li, and Singer (2009) occurred during solar minimum, when storms occur less frequently, and thus, such ULF wave events are likely less common.

While the superposed epoch signatures in activity were clear, they proved less pronounced in the solar wind. All quartiles show some enhancement in solar wind speed before the start of the event with the speed returning to background levels over the course of a couple of days. The enhanced speeds, however, are typically nowhere near as pronounced as the case study. The IMF tends to exhibit a small enhancement in magnitude and a tendency toward a slight southward component about a day before the start of events. No significant variations of the solar wind density with epoch time were found (not shown). The superposed epoch analysis, while showing clear evidence of storms beforehand, does not reveal clear overall signs of CMEs and/or magnetic clouds, which likely would remain even when considering the smearing out effects of the analysis. Given the clear signatures in activity (which would also be subject to the same smearing effect) but not in the solar wind, this suggests that the waves are predominantly driven via internal processes and it is likely that many geoeffective drivers, including, for instance, corotating interaction regions (e.g., Tsurutani et al., 2011), may also act as the causes of some of these ULF wave events. We leave a more detailed individual analysis of each event to future work.



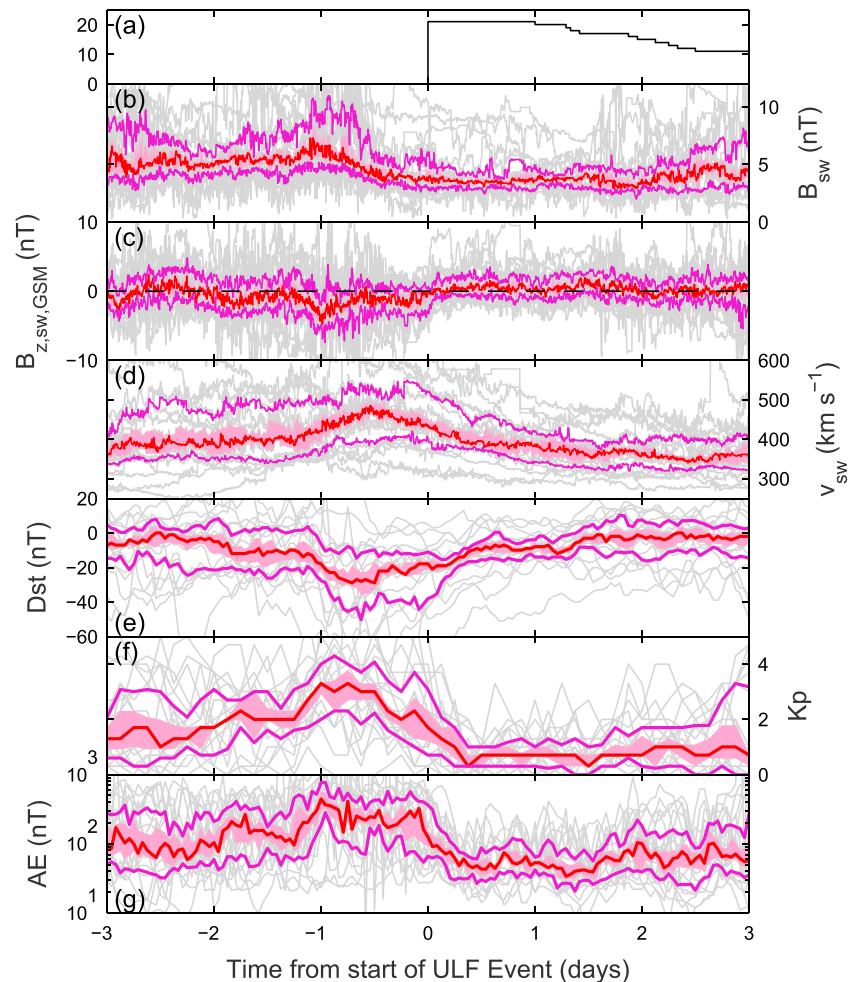


**Figure 6.** Superposed epoch analysis of the solar wind and geomagnetic conditions during the 21 identified ultralow-frequency (ULF) wave events. Displayed are the interplanetary magnetic field strength (b), interplanetary magnetic field GSM-z component (c), solar wind speed (d), and the (e) *Dst*, (f) *Kp*, and (g) *AE* geomagnetic activity indices. All time series are shown in gray with the medians (red) and corresponding standard error (red shaded) as well as interquartile ranges (purple) also displayed. Panel (a) indicates the number of ULF wave events occurring at each epoch time. GSM = geocentric solar magnetospheric.

#### 4. Conclusions

To potentially address some of the issues facing magnetospheric ULF wave research due to the big data being produced, we introduce sonification and citizen science. ULF waves were extracted from magnetometer data at geostationary orbit and converted into audible sound. This dramatically reduces the time frame for analysis and takes advantage of many of the benefits of the human auditory system compared to visual analysis (Divenyi, 2005; Hermann, 2002; Oppenheim & Magnasco, 2013; Robinson & Dadson, 1956; Whitton et al., 2014). We have shown that this sonified data can be used in exploratory citizen science, an approach somewhat different from typical citizen science projects.

The potential for the future use of sonification with citizen science has been demonstrated through the first results discovered by a group of London high school students. A case study event consisting of narrow-band waves of decreasing frequency spanning several days was found thanks to the citizen scientists' aural exploration of the data. These corresponded to second and fourth harmonic poloidal FLRs across the dayside magnetosphere. It was found that the event occurred during the recovery phase of a CME-driven geomagnetic storm. Simultaneous plasma density measurements revealed the initial erosion of magnetospheric plasma upon arrival of the CME and the subsequent refilling process. The identified frequencies of the observed waves agreed well with estimates of the field lines' eigenfrequencies made by combining these density

measurements throughout this refilling process with a magnetic field model, thereby explaining the frequencies throughout the event. These frequencies highly correlated with the solar wind speed and IMF strength to a degree much greater than usually expected, perhaps highlighting the importance of the storm phase and the time history of the magnetosphere in the empirical modeling of magnetospheric densities and FLR frequencies. We were able to rule out external driving mechanisms such as direct or resonant driving of the waves from the solar wind and excitation via the Kelvin-Helmholtz instability, concluding that the waves were likely driven by an internal process such as the ion bounce resonance (Glassmeier et al., 1999; Hughes et al., 1978; Southwood et al., 1969).

Events such as those presented in this manuscript are little discussed in the literature and had previously been reported as rare (Sarris, Li, & Singer, 2009; Sarris, Wright, & Li, 2009). However, by surveying the audio (and thus taking advantage of the human auditory system's pattern recognition and blind source separation abilities as well as the reduced time frame of the sonified data), we found this not to be the case. During 2013 alone, 21 events were discovered and superposed epoch analysis revealed that these tend to occur following storms, though no clear solar wind signature emerged. It may be possible that several different solar wind transients are capable of triggering such events. Further work is required to understand the range of driving conditions and properties of all of these events.

In conclusion, by combining sonification with citizen science it is possible to arrive at unexpected research results—The science results presented in this paper were possible only because of citizen scientists' unprescribed aural exploration of ULF wave data. Indeed, the MUSICS project was not set up with the particular class of ULF wave event presented in mind from the outset. Therefore, this approach has the potential to address some of the current challenges facing current magnetospheric ULF wave research. Sonified data could also be used within the more standard citizen science approach in the future, once a well-defined set of ULF wave event classifications and prescribed tasks for citizen scientists have been established. Given the potential benefits, the audible GOES ULF wave data set will now be made publicly available by NOAA. Finally, we hope that similar efforts become more widespread in the future and plan to implement them further across different data sets.

## Appendix A: Spectral Methods

Here we detail some of the spectral methods used that are well used in the fields of audio analysis but not widely applied in space physics.

### A.1. Pitch Detection

The autocorrelation of any periodic function is also a periodic function, exhibiting positive peak autocorrelation values of unity at lags given by integer multiples of the underlying period. Due to the finite length of real time series as well as the typical application of windowing functions, however, the height of these peaks in reality will decrease as the lag increases, reaching 0 when this equals the length of the window used. Here we present details of the autocorrelation pitch detection method used, which was based on that of Tolonen (2000) implemented within Audacity.

Autocorrelation functions were computed for 1,024-point Hanning windows of the (nondifferenced) magnetic field data, and we limit ourselves to positive lags only. Half-wave rectification was performed, whereby any negative autocorrelation values were set to zero, thereby leaving only a series of positive peaks in the case of a periodic signal. To remove repeated peaks originating from the same underlying periodicity, integer factor time-scaled copies of these autocorrelations were subtracted from the original. This was followed by again clipping to positive values only each time. This subtraction procedure was repeated for all prime numbers up to 11. The resulting function, named the Enhanced Summary Autocorrelation Function (ESACF) by Tolonen (2000), should leave positive peaks only at the fundamental periodicities of the signal.

Given the values of the ESACF peaks are not as simple to interpret as a standard autocorrelation, we specify two criteria for selecting significant peaks for each window of the data. First, we calculated the envelope function of the autocorrelation due to the Hanning window used. Our threshold for peaks in ESACF was chosen to be at least half that expected for perfect correlation. Second, we used a bootstrapping technique (Efron & Tibshirani, 1993), generating 25,000 realizations of 1,024-sample uncorrelated Gaussian white noise. The same windowing function was again applied, and the autocorrelations were calculated for each realization. At each lag, quantiles of the autocorrelations were computed to give a confidence interval for uncorrelated Gaussian

white noise. The  $1 - \alpha$  quantile at each lag corresponds to the local confidence level at the desired significance  $\alpha$ . However, we are performing multiple comparisons corresponding to the search for peaks present at any value of lag. Therefore, the global confidence level must be used to maintain the desired significance. We use the Bonferroni correction, which sets the confidence level to  $1 - \frac{\alpha}{N}$ , where  $N$  is the number of comparisons, that is, the length of the window in this case (Bonferroni, 1936; Dunn, 1958, 1961). We then required that the prominence (or intrinsic height) of peaks in ESACF be greater than the global 95% confidence level for uncorrelated Gaussian white noise.

## A.2. Welch's Method

Welch's overlapped averaged periodogram method (Stoica & Moses, 2005; Welch, 1967) is a way of estimating the power spectral matrix of a signal, reducing noise at the expense of frequency resolution. Each 1,024-sample set of data was split up into eight different data segments with 50% overlap. Hanning windows are then applied to each segment and the fast Fourier transform  $\mathcal{F}(x_i[t])$  computed for the windowed segments, where  $x_i[t]$  represents the segments of the original time series  $x[t]$ . In the case of autopower spectra, the periodograms for each segment are averaged together, which we denote by angular brackets with a subscript index  $\langle \mathcal{F}(x_i[t]) \mathcal{F}(x_i[t])^* \rangle_i$ , reducing the variance of the individual power measurements. For cross-spectra between  $x[t]$  and  $y[t]$ , the calculation is  $\langle \mathcal{F}(x_i[t]) \mathcal{F}(y_i[t])^* \rangle_i$ . Finally, the magnitude squared coherence using this method is given by

$$C_{xy} = \frac{\left| \langle \mathcal{F}(x_i[t]) \mathcal{F}(y_i[t])^* \rangle_i \right|^2}{\langle \mathcal{F}(x_j[t]) \mathcal{F}(x_j[t])^* \rangle_j \langle \mathcal{F}(y_k[t]) \mathcal{F}(y_k[t])^* \rangle_k} \quad (\text{A1})$$

## Acknowledgments

M. O. Archer thanks the students of Eltham Hill School who contributed to this study: Megan Wilkin, Hanan Mohamed, Isobel Currie, and David Perry and their teacher Russel Dobson. M. D. Hartinger was supported by NASA NNX17AD35G. We thank NOAA's National Centers for Environmental Information for access to GOES magnetometer data at <http://www.ngdc.noaa.gov/stp/satellite/goes/>. We acknowledge NASA contract NAS5-02099 and the THEMIS Mission, specifically J. W. Bonnell and F. S. Mozer for EFI data; C. W. Carlson and J. P. McFadden for ESA data; and K. H. Glassmeier, U. Auster, and W. Baumjohann for the use of FGM data provided under the lead of the Technical University of Braunschweig and with financial support through the German Ministry for Economy and Technology and the German Center for Aviation and Space (DLR) under contract 50 OC 0302. THEMIS data and analysis software (SPEDAS) are available at <http://themis.ssl.berkeley.edu>. The OMNI data were obtained from the NASA/GSFC OMNIWeb interface at <http://omniweb.gsfc.nasa.gov>. We thank the institutes who maintain the IMAGE Magnetometer Array: Tromsø Geophysical Observatory of UiT the Arctic University of Norway (Norway), Finnish Meteorological Institute (Finland), Institute of Geophysics Polish Academy of Sciences (Poland), GFZ German Research Centre for Geosciences (Germany), Geological Survey of Sweden (Sweden), Swedish Institute of Space Physics (Sweden), Sodankylä Geophysical Observatory of the University of Oulu (Finland), and Polar Geophysical Institute (Russia).

## References

- Agapitov, O., Glassmeier, K.-H., Auster, F. P. H.-U., Constantinescu, D., Angelopoulos, V., Magnes, W., et al. (2009). Surface waves and field line resonances: A THEMIS case study. *Journal of Geophysical Research*, *114*, A00C27. <https://doi.org/10.1029/2008JA013553>
- Alexander, R. L., Gilbert, J. A., Landi, E., Simoni, M., Zurbuchen, T. H., & Roberts, D. A. (2011). Audification as a diagnostic tool for exploratory heliospheric data analysis. In *The 17th International Conference on Auditory Display* (p. 1). Budapest, Hungary.
- Alexander, R. L., O'Modhrain, S., Roberts, D. A., Gilbert, J. A., & Zurbuchen, T. H. (2014). The bird's ear view of space physics: Audification as a tool for the spectral analysis of time series data. *Journal of Geophysical Research: Space Physics*, *119*, 5259–5271. <https://doi.org/10.1002/2014JA020025>
- Allan, W., White, S. P., & Poulter, E. M. (1986). Impulse excited hydromagnetic cavity and field-line resonances in the magnetosphere. *Planetary and Space Science*, *34*(4), 371–385. [https://doi.org/10.1016/0032-0633\(86\)90144-3](https://doi.org/10.1016/0032-0633(86)90144-3)
- Angelopoulos, V. (2008). The THEMIS mission. *Space Science Reviews*, *141*, 5–34. <https://doi.org/10.1007/s11214-008-9336-1>
- Angelopoulos, V. (2010). *The ARTEMIS mission* (pp. 3–25). New York, NY: Springer. [https://doi.org/10.1007/978-1-4614-9554-3\\_2](https://doi.org/10.1007/978-1-4614-9554-3_2)
- Archer, M. O. (2017). So you're looking to run a research in schools project? Practical tips from the evaluation of a pilot programme (Tech. rep.). London, UK: SEPnet. <https://doi.org/10.13140/RG.2.2.25674.06088>
- Archer, M. O., Hartinger, M. D., Walsh, B. M., & Angelopoulos, V. (2017). Magnetospheric and solar wind dependences of coupled fast-mode resonances outside the plasmasphere. *Journal of Geophysical Research: Space Physics*, *122*, 212–226. <https://doi.org/10.1002/2016JA023428>
- Archer, M. O., Hartinger, M. D., Walsh, B. M., Plaschke, F., & Angelopoulos, V. (2015). Frequency variability of standing Alfvén waves excited by fast mode resonances in the outer magnetosphere. *Geophysical Research Letters*, *42*, 10,150–10,159. <https://doi.org/10.1002/2015GL066683>
- Archer, M. O., & Plaschke, F. (2015). What frequencies of standing surface waves can the subsolar magnetopause support? *Journal of Geophysical Research*, *120*, 3632–3646. <https://doi.org/10.1002/2014JA020545>
- Arthur, C. W., McPherron, R. L., & Means, J. D. (1976). A comparative study of three techniques for using the spectral matrix in wave analysis. *Radio Science*, *11*(10), 833–845. <https://doi.org/10.1029/RS011i010p00833>
- Auster, H. U., Glassmeier, K. H., Magnes, W., Aydogar, O., Baumjohann, W., Constantinescu, D., et al. (2008). The THEMIS fluxgate magnetometer. *Space Science Reviews*, *141*, 235–264. <https://doi.org/10.1007/s11214-008-9365-9>
- Barkhausen, H. (1919). Two phenomena uncovered with help of the new amplifiers. *Zeitschrift für Physik*, *20*, 401–403.
- Barnard, L., Scott, C., Owens, M., Lockwood, M., Tucker-Hood, K., Thomas, S., et al. (2014). The solar stormwatch CME catalogue: Results from the first space weather citizen science project. *Space Weather*, *12*, 657–674. <https://doi.org/10.1002/2014SW001119>
- Bonferroni, C. E. (1936). Teoria statistica delle classi e calcolo delle probabilità. *Pubblicazioni del R Istituto Superiore di Scienze Economiche e Commerciali di Firenze*, *8*, 3–62.
- Bonnell, J. W., Mozer, F. S., Delory, G. T., Hull, A. J., Ergun, R. E., Cully, C. M., et al. (2008). The Electric Field Instrument (EFI) for THEMIS. *Space Science Reviews*, *141*, 303–341. <https://doi.org/10.1007/s11214-008-9469-2>
- Chaston, C. C. (2013). ULF waves and auroral electrons. In K. Takahashi, P. J. Chi, R. E. Denton, & R. L. Lysak (Eds.), *Magnetospheric ULF waves: Synthesis and new directions* (vol. 169, Geophysical Monograph Series. Washington, DC, USA: John Wiley & Sons, pp. 326. <https://doi.org/10.1029/169GM16>
- Chi, P. J., & Russell, C. T. (2008). Use of the Wigner-Ville distribution in interpreting and identifying ULF waves in triaxial magnetic records. *Journal of Geophysical Research*, *113*, A01218. <https://doi.org/10.1029/2007JA012469>
- Denton, R. E., Takahashi, K., Lee, J., Zeitler, C. K., Wimer, N. T., Litscher, L. E., et al. (2015). Field line distribution of mass density at geostationary orbit. *Journal of Geophysical Research*, *120*, 4409–4422. <https://doi.org/10.1002/2014JA020810>

- Divenyi, P. (Ed.) (2005). *Speech separation by humans and machines* Edited by Divenyi, P. Boston, MA: Springer Science + Business Media, Inc. <https://doi.org/10.1007/b99695>
- Dungey, J. W., & Southwood, D. J. (1970). Ultra low frequency waves in the magnetosphere. *Space Science Reviews*, 10(5), 672–688. <https://doi.org/10.1007/BF00171551>
- Dunn, O. J. (1958). Estimation of the means for dependent variables. *Annals of Mathematical Statistics*, 29, 1095–1111. <https://doi.org/10.1214/aoms/1177706374>
- Dunn, O. J. (1961). Multiple comparisons among means. *Journal of the American Statistical Association*, 56, 52–64. <https://doi.org/10.1080/01621459.1961.10482090>
- Efron, B., & Tibshirani, R. (1993). *An introduction to the bootstrap*. Boca Raton, FL: Chapman & Hall/CRC.
- Elkington, S. R. (2013). A review of ULF interactions with radiation belt electrons. In K. Takahashi, P. J. Chi, R. E. Denton, & R. L. Lysak (Eds.), *Magnetospheric ULF waves: Synthesis and new directions*, Geophysical Monograph Series (Vol. 169). Washington, DC: John Wiley & Sons. <https://doi.org/10.1029/169GM06>
- Ferradas, C. P., Zhang, J.-C., Spence, H. E., Kistler, L. M., Larsen, B. A., Reeves, G. D., et al. (2018). Temporal evolution of ion spectral structures during a geomagnetic storm: Observations and modeling. *Journal of Geophysical Research: Space Physics*, 123, 179–196. <https://doi.org/10.1002/2017JA024702>
- Glassmeier, K.-H., Buchert, S., Motschmann, U., Korth, A., & Pedersen, A. (1999). Concerning the generation of geomagnetic giant pulsations by drift-bounce resonance ring current instabilities. *Annales Geophysicae*, 17, 338–350. <https://doi.org/10.1007/s00585-999-0338-4>
- Green, C. A. (1985). Giant pulsations in the plasmasphere. *Planetary and Space Science*, 33(10), 1155–1168. [https://doi.org/10.1016/0032-0633\(85\)90073-X](https://doi.org/10.1016/0032-0633(85)90073-X)
- Harteringer, M. D., Moldwin, M. B., Zou, S., Bonnell, J. W., & Angelopoulos, V. (2015). ULF wave electromagnetic energy flux into the ionosphere: Joule heating implications. *Journal Geophysical Research*, 120, 494–510. <https://doi.org/10.1002/2014JA020129>
- Hermann, T. (2002). Sonification for exploratory data analysis (Master's thesis), Bielefeld University.
- Huang, N. E., Shen, Z., Long, S. R., Wu, M. C., Shih, H. H., Zheng, Q., et al. (1998). The empirical mode decomposition and the Hilbert spectrum for nonlinear and non-stationary time series analysis. *Proceedings of the Royal Society A*, 454, 903. <https://doi.org/10.1098/rspa.1998.0193>
- Hughes, W. J., & Southwood, D. J. (1976). The screening of micropulsation signals by the atmosphere and ionosphere. *Journal of Geophysical Research*, 81, 3,234–3,240. <https://doi.org/10.1029/JA081i019p03234>
- Hughes, W., Southwood, D. J., Mauk, B., McPherron, R. L., & Barfield, J. N. (1978). Alfvén waves generated by an inverted plasma energy distribution. *Nature*, 275, 43–45. <https://doi.org/10.1038/275043a0>
- Knipp, D. J. (2015). Space weather and citizen science. *Space Weather*, 13, 97–98. <https://doi.org/10.1002/2015SW001167>
- Korotova, G., Sibeck, D., Engebretson, M., Wygant, J., Thaller, S., Spence, H., et al. (2016). Multipoint spacecraft observations of long-lasting poloidal Pc4 pulsations in the dayside magnetosphere on 1–2 May 2014. *Annales Geophysicae*, 34, 985–998. <https://doi.org/10.5194/angeo-34-985-2016>
- Kramer, G. (1994). *An introduction to auditory display*. MA: Auditory Display: Sonification, Audification, and Auditory Interfaces, Addison-Wesley, Reading.
- Kunkel, T., & Reinhard, E. (2010). A reassessment of the simultaneous dynamic range of the human visual system. In *Proceedings of the 7th symposium on applied perception in graphics and visualization* (pp. 17–24). New York: ACM. <https://doi.org/10.1145/1836248.1836251>
- Lawrence, D. J., Thomsen, M. F., Borovsky, J. E., & McComas, D. J. (1999). Measurements of early and late time plasmasphere refilling as observed from geosynchronous orbit. *Journal Geophysical Research*, 104, 14,691–14,704. <https://doi.org/10.1029/1998JA900087>
- Le, G., Chi, P. J., Strangeway, R. J., Russell, C. T., Slavin, J. A., Takahashi, K., et al. (2017). Global observations of magnetospheric high-m poloidal waves during the 22 June 2015 magnetic storm. *Geophysical Research Letters*, 44, 3456–3464. <https://doi.org/10.1002/2017GL073048>
- MacDonald, E. A., Case, N. A., Clayton, J. H., Hall, M. K., Heavner, M., Lalone, N., et al. (2015). Aurorasaurus: A citizen science platform for viewing and reporting the aurora. *Space Weather*, 13, 548–559. <https://doi.org/10.1002/2015SW001214>
- Mann, I., Chisham, G., & Bale, S. D. (1998). Multisatellite and ground-based observations of a tailward propagating Pc5 magnetospheric waveguide mode. *Journal of Geophysical Research*, 103, 4657–4669. <https://doi.org/10.1029/97JA03175>
- Mann, I. R., O'Brien, T. K., & Milling, D. K. (2004). Correlations between ULF wave power, solar wind speed, and relativistic electron flux in the magnetosphere: Solar cycle dependence. *Journal of Atmospheric and Solar-Terrestrial Physics*, 66(2), 187–198. <https://doi.org/10.1016/j.jastp.2003.10.002>
- McFadden, J. P., Carlson, C. W., Bonnell, J., Mozer, F., Angelopoulos, V., Glassmeier, K. H., & Auster, U. (2008). THEMIS ESA first science results and performance issues. *Space Science Reviews*, 141, 447–508. <https://doi.org/10.1007/s11214-008-9433-1>
- McFadden, J. P., Carlson, C. W., Larson, D., Ludlam, M., Abiad, R., Elliott, B., et al. (2008). The THEMIS ESA plasma instrument and in-flight calibration. *Space Science Reviews*, 141, 277–302. <https://doi.org/10.1007/s11214-008-9440-2>
- McPherron, R. L. (2005). Magnetic pulsations: Their sources and relation to solar wind and geomagnetic activity. *Surveys in Geophysics*, 26, 545–592. <https://doi.org/10.1007/s10712-005-1758-7>
- Motoba, T., Takahashi, K., Rodriguez, J. V., & Russell, C. T. (2015). Giant pulsations on the afternoonside: Geostationary satellite and ground observations. *Journal of Geophysical Research: Space Physics*, 120, 8350–8367. <https://doi.org/10.1002/2015JA021592>
- Oppenheim, J. N., & Magnasco, M. O. (2013). Human time-frequency acuity beats the Fourier uncertainty principle. *Physical Review Letters*, 110, 44301. <https://doi.org/10.1103/PhysRevLett.110.044301>
- Piersanti, M., Materassi, M., Cicone, A., Spogli, L., Zhou, H., & Ezquer, R. G. (2018). Adaptive local iterative filtering: A promising technique for the analysis of nonstationary signals. *Journal Geophysical Research: Space Physics*, 123, 1031–1046. <https://doi.org/10.1002/2017JA024153>
- Robinson, D. W., & Dadson, R. S. (1956). A re-determination of the equal-loudness relations for pure tones. *British Journal of Applied Physics*, 7, 166.
- Rostoker, G., Lam, H.-L., & Olson, J. V. (1979). Pc 4 giant pulsations in the morning sector. *Journal Geophysical Research*, 84(A9), 5153–5166. <https://doi.org/10.1029/JA084iA09p05153>
- Samson, J. C., Jacobs, J. A., & Rostoker, G. (1971). Latitude-dependent characteristics of long-period geomagnetic micropulsations. *Journal Geophysical Research*, 76, 3675–3683. <https://doi.org/10.1029/JA076i016p03675>
- Sandhu, J. K., Yeoman, T. K., Fear, R. C., & Dandouras, I. (2016). A statistical study of magnetospheric ion composition along the geomagnetic field using the Cluster spacecraft for L values between 5.9 and 9.5. *Journal Geophysical Research*, 121, 2194–2208. <https://doi.org/10.1002/2015JA022261>
- Sarris, T., Li, X., & Singer, H. J. (2009). A long-duration narrowband Pc5 pulsation. *Journal Geophysical Research*, 114, A01213. <https://doi.org/10.1029/2007JA012660>



- Sarris, T. E., Wright, A. N., & Li, X. (2009). Observations and analysis of Alfvén wave phase mixing in the Earth's magnetosphere. *Journal Geophysical Research*, 114, A03218. <https://doi.org/10.1029/2008JA013606>
- Shue, J.-H., Song, P., Russell, C. T., Steinberg, J. T., Chao, J.-K., Zastenker, G., et al. (1998). Magnetopause location under extreme solar wind conditions. *Journal Geophysical Research*, 103, 17,691–17,700. <https://doi.org/10.1029/98JA01103>
- Singer, H. J., Southwood, D. J., Walker, R. J., & Kivelson, M. G. (1981). Alfvén wave resonances in a realistic magnetospheric magnetic field geometry. *Journal Geophysical Research*, 86, 4589–4596. <https://doi.org/10.1029/JA086iA06p04589>
- Smith, E. J., Holzer, R. E., McLeod, M. G., & Russell, C. T. (1967). Magnetic noise in the magnetosheath in the frequency range 3–300 Hz. *Journal Geophysical Research*, 72, 4803–4813. <https://doi.org/10.1029/JZ072i019p04803>
- Southwood, D. J. (1974). Some features of field line resonances in the magnetosphere. *Planetary and Space Science*, 22, 483–491. [https://doi.org/10.1016/0032-0633\(74\)90078-6](https://doi.org/10.1016/0032-0633(74)90078-6)
- Southwood, D. J., Dungey, J. W., & Etherington, R. J. (1969). Bounce resonant interaction between pulsations and trapped particles. *Planetary and Space Science*, 17(3), 349–361. [https://doi.org/10.1016/0032-0633\(69\)90068-3](https://doi.org/10.1016/0032-0633(69)90068-3)
- Stoica, P., & Moses, R. (2005). *Spectral analysis of signals*. NJ: Prentice Hall, Upper Saddle River.
- Takahashi, K., Denton, R. E., Hirahara, M., Min, K., Ohtani, S., & Sanchez, E. (2014). Solar cycle variation of plasma mass density in the outer magnetosphere: Magnetoseismic analysis of toroidal standing Alfvén waves detected by Geotail. *Journal of Geophysical Research: Space Physics*, 119, 8338–8356. <https://doi.org/10.1002/2014JA020274>
- Takahashi, K., Denton, R. E., Kurth, W., Kletzing, C., Wygant, J., Bonnell, J., et al. (2015). Externally driven plasmaspheric ULF waves observed by the Van Allen Probes. *Journal of Geophysical Research: Space Physics*, 120, 526–552. <https://doi.org/10.1002/2014JA020373>
- Takahashi, K., Denton, R. E., & Singer, H. J. (2010). Solar cycle variation of geosynchronous plasma mass density derived from the frequency of standing Alfvén waves. *Journal of Geophysical Research*, 115, A07207. <https://doi.org/10.1029/2009JA015243>
- Takahashi, K., Fennell, J. F., Amata, E., & Higbie, P. R. (1987). Field-aligned structure of the storm time Pc 5 wave of November 14–15. *Journal Geophysical Research*, 92, 5857–5864. <https://doi.org/10.1029/JA092iA06p05857>
- Takahashi, K., Lopez, R. E., McEntire, R. W., Zanetti, L. J., Kistler, L. M., & Ipavich, F. M. (1987). An eastward propagating compressional Pc5 wave observed by AMPTE/CCE in the postmidnight sector. *Journal Geophysical Research*, 92, 13,472–13,484. <https://doi.org/10.1029/JA092iA12p13472>
- Takahashi, K., Russel, C. T., & Anderson, R. R. (1985). ISEE 1 and 2 observation of the spatial structure of a compressional Pc 5 wave. *Geophysical Research Letters*, 12, 63. <https://doi.org/10.1029/GL012i009p00613>
- Takahashi, K., Yumoto, K., Claudepierre, S. G., Sanchez, E. R., Troshichev, O. A., & Janzhura, A. S. (2012). Dependence of the amplitude of Pc5-band magnetic field variations on the solar wind and solar activity. *Journal of Geophysical Research*, 117, A04207. <https://doi.org/10.1029/2011JA017120>
- Tamao, T. (1965). Transmission and coupling resonance of hydromagnetic disturbances in the non-uniform Earth's magnetosphere. *The science reports of the Tohoku University series*, 5, 44–72.
- Tolonen, T. (2000). A computationally efficient multipitch analysis model. *IEEE Transactions on Speech and Audio Processing*, 8(6), 708–716. <https://doi.org/10.1109/89.876309>
- Tsurutani, B. T., Lakhina, G. S., Verkhoglyadova, O. P., Gonzalez, W. D., Echer, E., & Guarnieri, F. L. (2011). A review of interplanetary discontinuities and their geomagnetic effects. *Journal of Atmospheric and Solar-Terrestrial Physics*, 73, 5–19. <https://doi.org/10.1016/j.jastp.2010.04.001>
- Tsyganenko, N. A. (1995). Modeling the Earth's magnetospheric magnetic field confined within a realistic magnetopause. *Journal of Geophysical Research*, 100, 5599–5612. <https://doi.org/10.1029/94JA03193>
- Tsyganenko, N. A. (1996). Effects of the solar wind conditions in the global magnetospheric configurations as deduced from data-based field models. In E. Rolfe & B. Kaldeich (Eds.), *International conference on substorms, proceedings of the 3rd International Conference held in Versailles*. Paris: European Space Agency, pp. 181.
- Urban, K. D., Gerrard, A. J., Lanzerotti, L. J., & Weatherwax, A. T. (2016). Rethinking the polar cap: Eccentric dipole structuring of ULF power at the highest corrected geomagnetic latitudes. *Journal of Geophysical Research: Space Physics*, 121, 8475–8507. <https://doi.org/10.1002/2016JA022567>
- Ville, J. (1948). Théorie et applications de la notion de signal analytique. *Câbles et Transmission*, 2, 61–74.
- Welch, P. D. (1967). The use of fast Fourier transform for the estimation of power spectra: A method based on time averaging over short, modified periodograms. *IEEE Transactions on Audio and Electroacoustics*, 15, 70–73. <https://doi.org/10.1109/TAU.1967.1161901>
- Whitton, J. P., Hancock, K. E., & Polley, D. B. (2014). Immersive audiomotor game play enhances neural and perceptual salience of weak signals in noise. In N. J. Kopell (Ed.), *Proceedings of the National Academy of Sciences of the United States of America*. Washington, DC: National Academy of Sciences of the United States of America. <https://doi.org/10.1073/pnas.1322184111>
- Wicks, R. T., Alexander, R. L., Stevens, M., Wilson, L. B. III, Moya, P. S., Viñas, A., et al. (2016). A proton-cyclotron wave storm generated by unstable proton distribution functions in the solar wind. *The Astrophysical Journal*, 819(1), 6. <https://doi.org/10.3847/0004-637X/819/1/6>
- Wigner, E. (1932). On the quantum correction for thermodynamic equilibrium. *Physical Review*, 40, 749. <https://doi.org/10.1103/PhysRev.40.749>
- Wilcoxon, F. (1945). Individual comparisons by ranking methods. *Biometrics Bulletin*, 1, 80–83. <https://doi.org/10.2307/3001968>
- Wright, A. N., & Mann, I. R. (2006). Global MHD eigenmodes of the outer magnetosphere. In K. Takahashi, P. J. Chi, R. E. Denton, & R. L. Lysak (Eds.), *Magnetospheric ULF waves: Synthesis and new directions* (vol. 169), Geophysical Monograph Series. Washington, DC, USA: John Wiley & Sons, pp. 51. <https://doi.org/10.1029/169GM06>